

Extension of the flux fit method

Extension of the flux fit method for estimating power deposition profiles

J.H. Slief,^{1,2} R.J.R. van Kampen,^{1,3} M.W. Brookman,⁴ and M. van Berkel¹

¹*DIFFER - Dutch Institute for Fundamental Energy Research, De Zaal 20, 5612 AJ Eindhoven, the Netherlands*

²*Science and Technology of Nuclear Fusion, Department of Applied Physics, Eindhoven University of Technology, P.O. Box 513, 5600 MB Eindhoven, the Netherlands*

³*Control Systems Technology, Department of Mechanical Engineering, Eindhoven University of Technology, P.O. Box 513, 5600 MB Eindhoven, the Netherlands*

⁴*General Atomics, 3550 General Atomics Ct, San Diego, California 90005, USA*

(*Electronic mail: J.H.Slief@diffier.nl)

(Dated: 24 December 2021)

The flux fit method is used to self-consistently estimate the power deposition profile and heat transport profiles from temperature measurements originating from perturbative experiments with a modulated source. This letter improves on this method by addressing the limitations and assumptions. The most crucial improvement is the additional freedom in the source deposition profile. Allowing for a variable central deposition location and height and including a skewness parameter produces deposition profiles more consistent with the measurement data, but still wider than equilibrium ray tracing in two different DIII-D discharges. Moreover, we show that the quality of the estimated deposition profile is key to the accuracy of diffusivity and convectivity estimates, but inversely, the estimated transport parameters hardly affect the quality of the power deposition estimate. Using this method, we show that the power deposition profile estimate is broadened with respect to ray-tracing by about 1.7-1.8 times in two DIII-D discharges.

The application of RF power in the electron cyclotron (EC) range of frequencies to a tokamak plasma results in particularly localized resonance, with high power EC waves playing a crucial role in stabilizing plasma instabilities such as neoclassical tearing modes (NTMs) by driving current within magnetic island structures as small as a few centimeters wide¹. Recent studies have demonstrated that interactions between the propagating wave and plasma turbulence before it reaches any resonance can have a significant impact on the deposition profiles of the RF wave², with potential implications for e.g. NTM control in ITER³. However, resolving this effect from plasma processes is a significant challenge. Fast transport in response to applied heating power can obscure the width of the power deposition profile⁴. Determining the full deposition profile therefore requires self-consistent treatment of applied power and the resulting transport^{5,6}. To this end, Brookman et al. developed a method to self-consistently estimate power deposition and transport profiles from temperature measurements in response to a modulated RF heating source, denoted here as the 'flux fit method'⁷.

This letter presents a set of tools which improve on this method by addressing limitations and assumptions, which include limited freedom in the deposition profile estimation. With this set of tools, the method could prove valuable in assessing EC wave launcher performance and the controllability of MHD instabilities like NTMs, where the power deposition width in relation to the island width is a crucial control parameter⁸. Moreover, the tools are capable of being run on a large data sets rapidly, allowing the benchmarking of simulations that include turbulence broadening and the development of predictive models of deposition broadening.

Before starting to introduce our extended methodology, We briefly re-visit the flux fit method presented in Ref.⁷ on which our extension is built. The original method, and our extended method, are based on the use of:

1. spatially and temporally resolved temperature perturbation measurements $\tilde{T}(\rho, t)$ resulting from a known modulated heat source $\tilde{U}(t)$,
2. a Gaussian parametrization of the (modulated part of the) expected source deposition profile $P_M(\rho)$,

with time t , $\rho = \sqrt{\psi_N}$ the square root of normalized toroidal flux (often referred to as 'normalized minor radius' and typically well approximated by $\rho \approx \frac{r}{a}$, with plasma minor radius a and r the distance from the magnetic axis).

The main difference between the work presented in this letter and in Ref.⁷ is the freedom in the source profile parametrization, which also has consequences for the optimization.

In Ref.⁷, the structure of the deposition profile is taken as a Gaussian fit of the TORAY-GA⁹ ray-tracing profile. The resulting profile is convoluted with a Gaussian filter which results in a Gaussian profile at the same peak location that is broadened by a (variable) factor b . This factor b is taken as a free parameter that is varied to determine the deposition profile $P(\rho, b)$. To determine the best fit for b , an iterative two-step procedure is used which involves calculating the perturbed heat-flux $\tilde{Q}(\rho, \omega)$ directly resulting from the modulated source:

$$\tilde{Q}(\rho, \omega) = \frac{1}{\rho} \int_0^\rho \rho' \left(\frac{3i}{2} \omega n(\rho') \tilde{\Theta}(\rho', \omega) - P_M(\rho', b) \tilde{\Upsilon}(\omega) \right) d\rho', \quad (1)$$

in cylindrical geometry^{4,10}, where density $n(\rho)$ is assumed to be time-invariant and unaffected by the source perturbation but allowed to vary spatially. $\tilde{\Theta}(\omega, \rho) = \mathcal{F}\{\tilde{T}(\rho, t)\}$ is the Fourier transform of the measured $\tilde{T}(\rho, t)$, $\tilde{\Upsilon}(\omega) = \mathcal{F}\{\tilde{U}(t)\}$ and $\tilde{Q}(\rho, \omega)$ the resulting (perturbed) heat flux in the frequency domain. This formulation of the flux is fit to a

Extension of the flux fit method

diffusive-convective model plus a coupled transport term ξ dependent on the density modulation $\tilde{v}(\rho, \omega) = \mathcal{F}\{\tilde{n}(\rho, t)\}$:

$$\tilde{Q}(\omega)/n = -D_M \nabla_\rho \tilde{\Theta}(\omega) + V_M \tilde{\Theta}(\omega) + \xi(\omega, \tilde{v}), \quad (2)$$

where all terms are dependent on ρ , so this dependency has been omitted for the sake of brevity. This fit is made for several values of b where the best fit belongs to the minimum of the fit residual χ^2 .

Given that only b needs to be optimized, this optimization approach is feasible. However, the use of a single free parameter places a severe restriction on the shape of profiles that can be estimated. Therefore, we propose an extension of the number of free parameters. With this, the total parameter space to be covered quickly explodes, such that a new optimization procedure is needed.

The new source profile parametrization is defined as:

$$P_M(\rho, b, \zeta, A, \alpha) = R(\rho, b, \zeta, A)S(\rho, \alpha), \quad (3)$$

which is comprised of the product of two functions R and S and contains four free parameters (b, ζ, A, α). R is obtained from the expected source profile by fitting a Gaussian to the TORAY estimation like in Ref.⁷ and adding the free parameters b, ζ and A :

$$R(\rho, b, \zeta, A) = A \exp\left(-\left(\frac{\rho - (\mu_{\text{TORAY}} - \zeta)}{b\sigma_{\text{TORAY}}}\right)^2\right), \quad (4)$$

The parameters b and ζ are included to account for shifted and broadened profiles while the freedom in the parameter A removes the need for a-priori assumptions on the amount of power absorbed. This latter parameter currently serves as a consistency check but in the future could be used to detect power losses in the EC system, for instance due to significant shine-through.

To account for non-symmetric profiles (see e.g.^{11,12}), R is multiplied by a skew function S with parameter α , given by:

$$S(\rho, \alpha) = 1 + \operatorname{erf}\left(\alpha \left(\frac{\rho - \mu}{\sqrt{2}\sigma_F}\right)\right), \quad (5)$$

where erf denotes the error function and $\mu = \mu_{\text{TORAY}} - \zeta$.

To find the optimal fit for (3), we no longer make use of the two-step approach as in Ref.⁷, since there are too many combinations of four fit parameters to pick them from a grid of possible values. Instead, we use an iterative nonlinear least squares approach that fits $D_M(\rho)$, $V_M(\rho)$ and $\xi(\rho)$, parametrized either by polynomials of arbitrary order or third-degree B-splines, to the parametrization of the perturbed heat flux $\tilde{Q}(\rho, \omega, b, \zeta, A, \alpha)$:

$$\chi^2 = \min_{x,y} \left\| \tilde{Q}(\rho, \omega, x) - y[\nabla_\rho \tilde{\Theta}(\rho, \omega), \tilde{\Theta}(\rho, \omega), 1]^T \right\|^2, \quad (6)$$

with the (optimal) solutions $x = [b, \zeta, A, \alpha]$ and $y = [D_M(\rho), V_M(\rho), \xi(\rho)]$ and χ^2 the (squared) fit residual

2

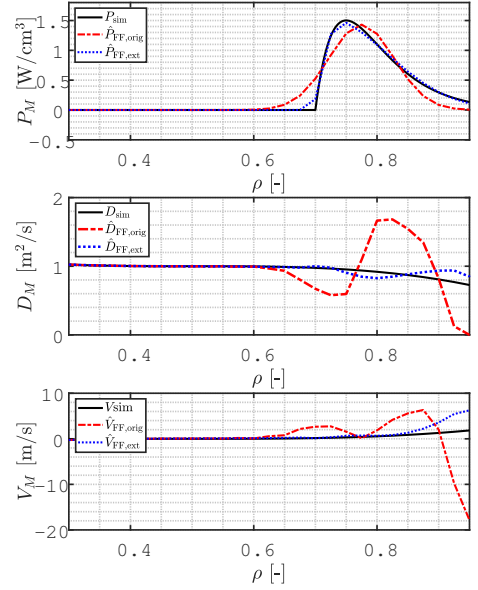


FIG. 1: Estimation of power deposition, diffusivity and convectivity profiles from a simulation (shown in black) of a perturbation experiment with $\tilde{q}_r^{\text{sim}}(\rho, t) = -D_M^{\text{sim}}(\rho)\nabla_\rho \tilde{T}(\rho, t) + V_M^{\text{sim}}(\rho)\tilde{T}(\rho, t)$, where $D_M^{\text{sim}}(\rho) = -3(\rho - 0.5)^3 + 1$, $V_M^{\text{sim}}(\rho) = 30(\rho - 0.5)^3$ and $P_M^{\text{sim}}(\rho) = 52 * \max(\sin(0.5\pi(\rho - 0.7)), 0) e^{(-20(\rho - 0.7) + 0.05)}$, comparing the resulting estimates from the original flux fit method⁷ (denoted by FF,orig and shown in red dashes) to the extended flux fit method presented in this letter (denoted by FF,ext and shown in blue dots).

given x and y . The nonlinear optimization (6) is performed using the trust-region-reflective algorithm^{13,14}, and it is performed simultaneously across (a chosen number of) the perturbed frequencies ω .

We validate the extended estimation method by applying it to a set of simulated data and comparing with the original method with only a single free parameter in the source profile, b .

A set of temperature perturbation data was generated using the models (1), (2) and artificial profiles for power deposition, diffusivity and convectivity. See figure 1. The P_M profile is a skewed, non-Gaussian function consisting of the positive part of a sine wave plus an exponential decay (see caption of fig. 1). The diffusivity and convectivity profiles are generated using third-order polynomials and are estimated using B-splines.

The estimation results for the original and extended methods are, respectively, shown in figure 1 in red dash-dots and blue dots. From the figure it becomes clear that errors made

Extension of the flux fit method

3

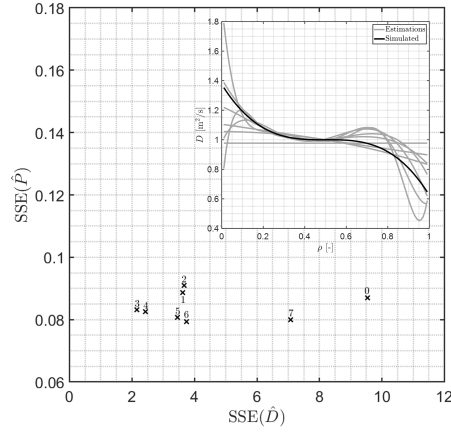


FIG. 2: Sum of squared errors (SSE) as defined by (7) of the extended flux fit power deposition estimation compared to a simulated profile like that of fig. 1, as a function of the diffusivity SSE for polynomial D_M estimations of order varying between 0 and 7. The simulated and estimated D_M profiles are shown in the top right of the figure. The residual error between the estimated and simulated power deposition profiles is small and nearly independent of the accuracy of the diffusivity estimation.

in the estimation of the deposition profile need to be compensated by the transport profiles, that subsequently deviate significantly from the 'true' (i.e. simulated) profiles. Moreover, due to the spatial integral definition of the flux that is fit (equation 1), discrepancies between the estimated and intrinsic deposition profiles also get integrated and the deviation of the transport estimates from the intrinsic profiles grows with radius. Due to this effect, it is hard to accurately estimate diffusivity and convectivity profiles with this method. This, however, is found to be largely inconsequential to accurate source profile estimations. To support this, the sum of squared errors (SSE) between the estimated source profile using the extended flux fit method and the simulated profile was plotted against the SSE between the estimated diffusivity and the simulated profile, for polynomial orders of the estimated diffusivity profile ranging between 0 (constant over the entire domain) and 7. The SSE is defined by:

$$\text{SSE}(\hat{X}^{\text{Flux fit}}) = \sum_i^n (X^{\text{sim}}(\rho_i) - \hat{X}^{\text{Flux fit}}(\rho_i))^2, \quad (7)$$

where X^{sim} is the simulated profile, i.e. D_M^{sim} or P_M^{sim} , $\hat{X}^{\text{Flux fit}}$ is the flux fit estimation of that same profile, n is the total number of spatial points and ρ_i is the i th spatial point.

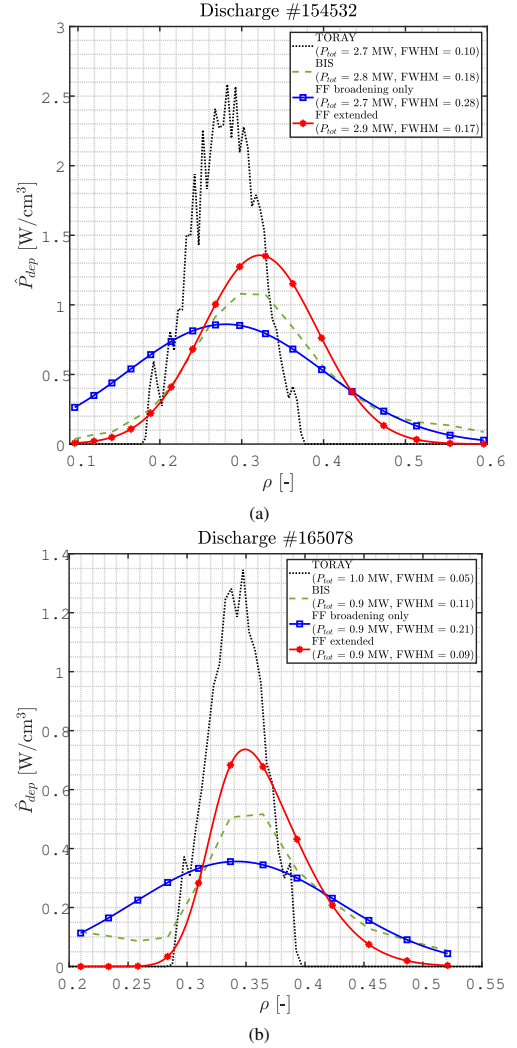


FIG. 3: Estimation of the power density deposited by modulated Electron Cyclotron Heating (ECH) as a function of normalized minor radius $\rho \approx r/a$ in DIII-D discharges (a) 154532 and (b) 165078. The broadening-only implementation of the flux fit method (FF broadening only) shows a broadened deposition profile compared to the TORAY-GA⁹ ray tracing estimate. The extended flux fit method (FF extended), presented in this work, shows a less severe broadening by allowing for a freedom in the peak location and (b) a skewed profile. A break-in-slope (BIS) estimate is shown for comparison.

Extension of the flux fit method

4

The result, shown in fig. 2, shows that the accuracy of the source (P_M) estimation is independent of the accuracy of the diffusivity (D_M) estimation. This implies that, provided we have sufficient freedom in the estimation of P_M , we can accurately estimate the deposition profile. However, errors made in the estimation thereof are compensated through the transport estimation, i.e., affect the estimated D_M and V_M . This supports earlier findings¹⁵. Hence, the estimated D_M and V_M profiles will not necessarily reflect the intrinsic transport profiles and have little influence on the estimated deposition profile. Inversely, this implies that large errors made in the estimation of D_M and V_M reflect errors made in the estimation of P_M . With prior knowledge of intrinsic transport profiles, any discrepancy between them and the estimated profiles provides a hint that the estimated deposition profile might deviate from the intrinsic one. Without any such prior knowledge, large values (say, $D_M \gtrsim 1 \text{ m}^2/\text{s}$ and $|V_M| \gtrsim 10 \text{ m/s}$ in a DIII-D-sized tokamak) might provide the same.

After verification of the method in simulation, the extended flux fit method is applied to two datasets from DIII-D: discharges 154532 (limited L-mode, $B_t = 2.0 \text{ T}$, $I_p = 1.2 \text{ MA}$, $n_{e,0} = 4.2 \times 10^{19} \text{ m}^{-3}$, $P_{\text{inj, mod}} = 3.0 \text{ MW}$ and $f_{\text{mod}} = 50 \text{ Hz}$) and 165078 (diverted L-mode, $B_t = 2.0 \text{ T}$, $I_p = 1.0 \text{ MA}$, $n_{e,0} = 2.9 \times 10^{19} \text{ m}^{-3}$, $P_{\text{inj, mod}} = 1.0 \text{ MW}$ and $f_{\text{mod}} = 70 \text{ Hz}$), both analyzed in Ref.⁷. Power is applied to the plasma by Electron Cyclotron Heating (ECH) and modulated between 10 and 100% power. Fast Electron Cyclotron Emission (ECE) data (sampled at 500 kHz) is used to measure the resulting electron temperature perturbations through 40 channels corresponding to different spatial locations. Electron density measurements are provided by the DIII-D Thomson scattering diagnostic.

We apply and compare the following four power deposition estimation methods to the above discharges:

- TORAY-GA⁹,
- The extended flux fit method,
- The flux fit method where only b is varied (denoted by FF broadening only), to mimic the method as implemented by Brookman et al.⁷
- Break-in-slope¹⁶, as a reference for the two flux fit methods.

For discharge 154532 the first 5 and for discharge 165078 the first 3 harmonics of the modulation frequency were used in the flux fit estimations, corresponding to a signal-to-noise ratio (SNR) of $\geq 10 \text{ dB}$. Moreover, the Local Polynomial Method (LPM) is used to remove trends from the measured temperature signals in the frequency domain¹⁷. Figure 3 shows the results.

Figure 3a shows the importance of allowing the freedom of peak location. The broadening-only method (denoted by the squares) is fixed in its peak location and can therefore only compensate for an apparent shift in peak power deposition location in the measurement data with respect to the TORAY estimation by substantial broadening. This shift could arise due

to a variety of reasons, including deviations from local power absorption conditions in TORAY due to the power levels injected, plasma edge events temporarily shifting the TORAY estimated peak at the timestamp the profile was computed or inaccuracies in the mapping of temperature measurements to ρ . We define the broadening factor β as the ratio of full width at half maximum¹⁸ (FWHM) of the flux fit estimate to the FWHM of the TORAY estimate (FWHM_{TORAY}):

$$\beta = \text{FWHM}/\text{FWHM}_{\text{TORAY}}, \quad (8)$$

such that the broadening factor $\beta = 1$ when both curves are equally wide, $\beta > 1$ when the flux fit estimate is broader than the TORAY estimate and $\beta < 1$ when the flux fit estimate is less broad.

The broadening-only estimate shows a broadening of $\beta = 2.8$ over TORAY. The extended method finds a peak position shifted about 0.06 in ρ (corresponding to about 4 cm in DIII-D) to the right. This peak position coincides with the peak estimated by the break-in-slope method (shown for reference as the dashed line), which is a method independent of any initial estimate of the profile. With the shift in peak position, the broadening with respect to the TORAY estimate is significant, but drastically reduced from $\beta = 2.8$ to 1.7. The fit residual, defined by (6), is also reduced from $\sqrt{\chi^2} = 0.0218 \text{ W/cm}^3$ for the broadening-only fit to only 0.0099 W/cm^3 for the extended flux fit estimate. This 2.2 times reduction in fit residual indicates that the additional freedom in central deposition location provides a fit more consistent with the measurement data compared to allowing only the width to vary.

The importance of including the skew parameter α in combination with a variable peak location is illustrated in figure 3b. In this particular case, where the best fit using the extended flux fit method gives a skewness value $\alpha \approx 4$, allowing for a non-symmetric profile significantly reduces the broadening needed to fit the measurement data. Again, a significant broadening with respect to the ray tracing estimate as observed in⁷ remains, yet is considerably reduced from $\beta = 4.2$ when only the broadening is allowed to be varied to $\beta = 1.8$ in the extended method with all four parameters. The fit residual $\sqrt{\chi^2}$ is likewise reduced from 0.0067 W/cm^3 in the broadening-only fit to 0.0045 W/cm^3 in the extended flux fit estimate, a reduction of 1.5 times.

Note that Brookman et al. report a broadening of 2.2 according to the definition in (8) for this discharge⁷, which deviates from the 4.2 broadening factor for the broadening-only method in figure 3b. This is expected to be due to the differences in fitting and optimization routines: orthogonal distance regression (ODR) in Ref.⁷ versus iterative nonlinear least squares. We have also checked our results against a (time-consuming) grid search algorithm. The result is very close to our gradient descent result validating that the algorithm found a minimum close to the global minimum. The small difference is caused by a numerical approximation of the Jacobian, which in the future will be replaced by an analytic implementation likely resolving the small differences.

Extension of the flux fit method

5

For completeness, we also want to note that there are alternative (exotic) explanations for a broadening effect due to fast non-local transport mechanisms. Theoretically, this would also lead to an apparent broadening of the deposition profile as estimated using the methodologies presented here¹⁰.

In conclusion, this work presents an extension to the 'flux fit' method⁷ for estimating power deposition profiles and spatially varying modulated heat transport coefficients based on temperature measurements from a periodically perturbed source and a parametrization of its expected spatial profile. In this work, the number of parameters available for fitting of the source function is extended to include a variable peak location, peak height, and a skewness parameter. Because of this, the optimization procedure is therefore changed to a nonlinear least squares optimization.

The (extended) flux fit method serves as a clear improvement over traditional methods for experimentally determining the deposition profile^{9,19}, due to the self-consistent treatment of power deposition and transport. This reduces the transport broadening of the observed deposition profile that has traditionally plagued these methods. The downside is a slightly higher computational cost.

The method is applied to DIII-D discharges 154532 and 165078 (see Ref.⁷) to show that there is a significant broadening compared to ray tracing, but considerably reduced compared to the original publication. In both discharges, the fits from our method are more consistent with the measurement data than the broadening-only fits.

It is shown that the method is very suitable for power deposition estimates but not for accurate transport profile estimations. It can be used to further understand deposition broadening and how this might impact profile- and instability control in devices like ITER and DEMO.

I. ACKNOWLEDGEMENTS

This work has been carried out within the framework of the EUROfusion Consortium and has received funding from the Euratom research and training programme 2014-2018 and 2019-2020 under grant agreement No 633053. The views and opinions expressed herein do not necessarily reflect those of the European Commission.

Data used in this publication was generated in experiments funded by the US Department of Energy under DE-FC02-04ER54698.

II. DISCLAIMER

This report was prepared as an account of work sponsored by an agency of the United States Government. Neither the United States Government nor any agency thereof, nor any of their employees, makes any warranty, express or implied, or assumes any legal liability or responsibility for the accuracy, completeness, or usefulness of any information, appa-

ratus, product, or process disclosed, or represents that its use would not infringe privately owned rights. Reference herein to any specific commercial product, process, or service by trade name, trademark, manufacturer, or otherwise, does not necessarily constitute or imply its endorsement, recommendation, or favoring by the United States Government or any agency thereof. The views and opinions of authors expressed herein do not necessarily state or reflect those of the United States Government or any agency thereof.

DATA AVAILABILITY STATEMENT

Raw data were generated at the DIII-D tokamak. Derived data supporting the findings of this study are available from the corresponding author upon reasonable request.

¹G. Gantenbein, H. Zohm, G. Giruzzi, S. Günter, F. Leuterer, M. Maraschek, J. Meskat, and Q. Yu, *Physical Review Letters* **85**, 1242 (2000).

²O. Chellaï, S. Alberti, M. Baquero-Ruiz, I. Furno, T. Goodman, F. Manke, G. Plyushchev, L. Guidi, A. Koehn, O. Maj, E. Poli, K. Hizanidis, L. Figini, and D. Ricci, *Physical Review Letters* **120**, 105001 (2018).

³E. Poli, C. Angioni, F. Casson, D. Farina, L. Figini, T. Goodman, O. Maj, O. Sauter, H. Weber, H. Zohm, G. Saibene, and M. Henderson, *Nuclear Fusion* **55**, 013023 (2015).

⁴U. Stroth, L. Giannone, and H. J. Hartfuss, *Plasma Physics and Controlled Fusion* **38**, 611 (1996).

⁵M. van Berkel, T. Kobayashi, G. Vandersteen, H. J. Zwart, H. Igami, S. Kubo, N. Tamura, H. Tsuchiya, and M. R. de Baar, *Nuclear Fusion* **58**, 096036 (2018).

⁶K. W. Gentile, M. E. Austin, J. C. Deboo, T. C. Luce, and C. C. Petty, *Physics of Plasmas* **13**, 1 (2006).

⁷M. W. Brookman, M. E. Austin, C. C. Petty, R. J. La Haye, K. Barada, T. L. Rhodes, Z. Yan, A. Köhn, M. B. Thomas, J. Leddy, and R. G. L. Vann, *Physics of Plasmas* **28**, 42507 (2021).

⁸B. Hennen, E. Westerhof, P. Nuij, M. de Baar, and M. Steinbuch, *Nuclear Fusion* **52**, 074009 (2012).

⁹R. Prater, D. Farina, Y. Gribov, R. W. Harvey, A. K. Ram, Y. R. Lin-Liu, E. Poli, A. P. Smirnov, F. Volpe, E. Westerhof, and A. Zvonkov, *Nuclear Fusion* **48**, 035006 (2008).

¹⁰M. van Berkel, G. Vandersteen, H. J. Zwart, G. M. Hogeweij, J. Citrin, E. Westerhof, D. Peumans, and M. R. de Baar, *Nuclear Fusion* **58**, 17 (2018).

¹¹E. Westerhof, *Electron cyclotron waves, transport and instabilities in hot plasmas*, Ph.D. thesis, Rijksuniversiteit te Utrecht (1987).

¹²E. Westerhof and W. J. Goedheer, *Plasma Physics and Controlled Fusion* **30**, 1691 (1988).

¹³T. Coleman and Y. Li, *Mathematical Programming* **67**, 189 (1994).

¹⁴T. F. Coleman and Y. Li, *SIAM Journal on Optimization* **6**, 418 (1996).

¹⁵M. van Berkel, G. W. Oosterwegel, G. Vandersteen, H. J. Zwart, G. Hogeweij, E. Westerhof, and J. Citrin, in *46th European Physical Society Conference on Plasma Physics (EPS 2019)* (Milan, 2019).

¹⁶E. A. Lerche and D. Van Eester, *Plasma Physics and Controlled Fusion* **50**, 035003 (2008).

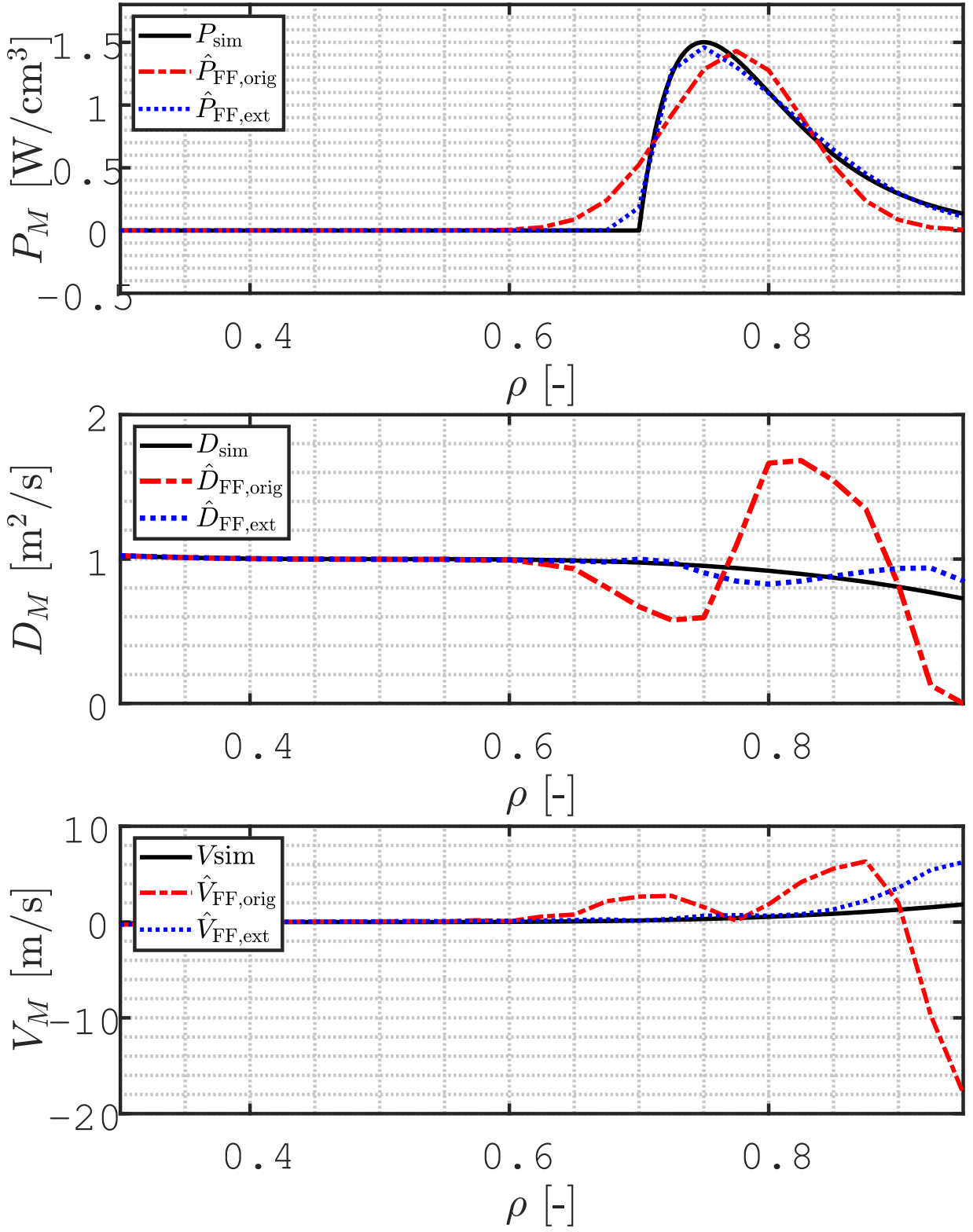
¹⁷M. van Berkel, R. J. R. van Kampen, G. Vandersteen, T. Kobayashi, T. Ravensbergen, H. Igami, J. T. Lammers, G. W. Oosterwegel, C. Galperti, F. Felici, and M. R. de Baar, *Plasma Physics and Controlled Fusion* **62**, 094001 (2020).

¹⁸M. H. Weik, *full-width at half-maximum*, in *Computer Science and Communications Dictionary* (Springer US, Boston, MA, 2001) pp. 661–661.

¹⁹K. K. Kirov, F. Leuterer, G. V. Pereverzev, F. Ryter, and W. Suttrop, *Plasma Physics and Controlled Fusion* **44**, 2583 (2002).

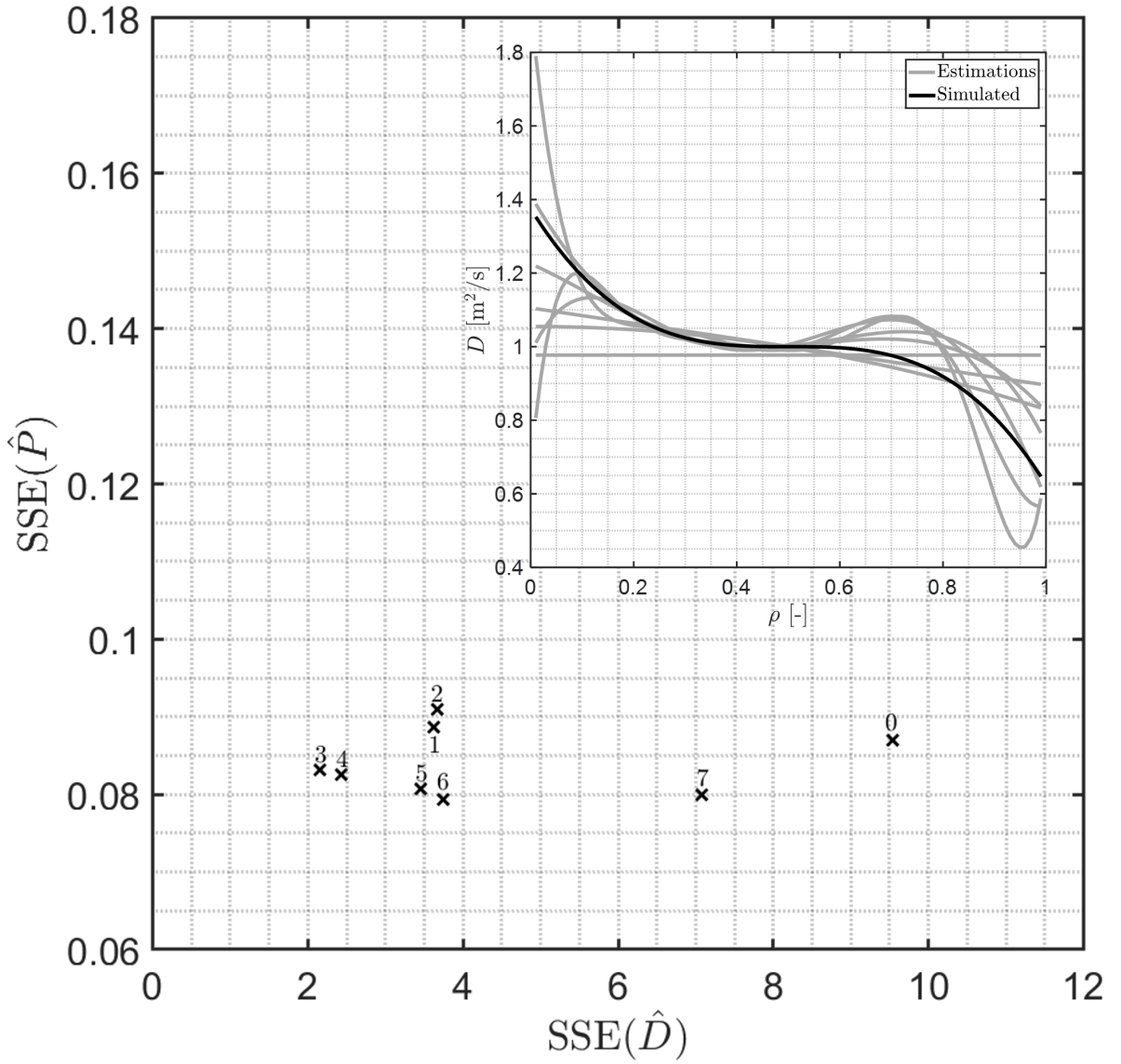
This is the author's peer reviewed, accepted manuscript. However, the online version of record will be different from this version once it has been copyedited and typeset.

PLEASE CITE THIS ARTICLE AS DOI: 10.1063/5.0069869



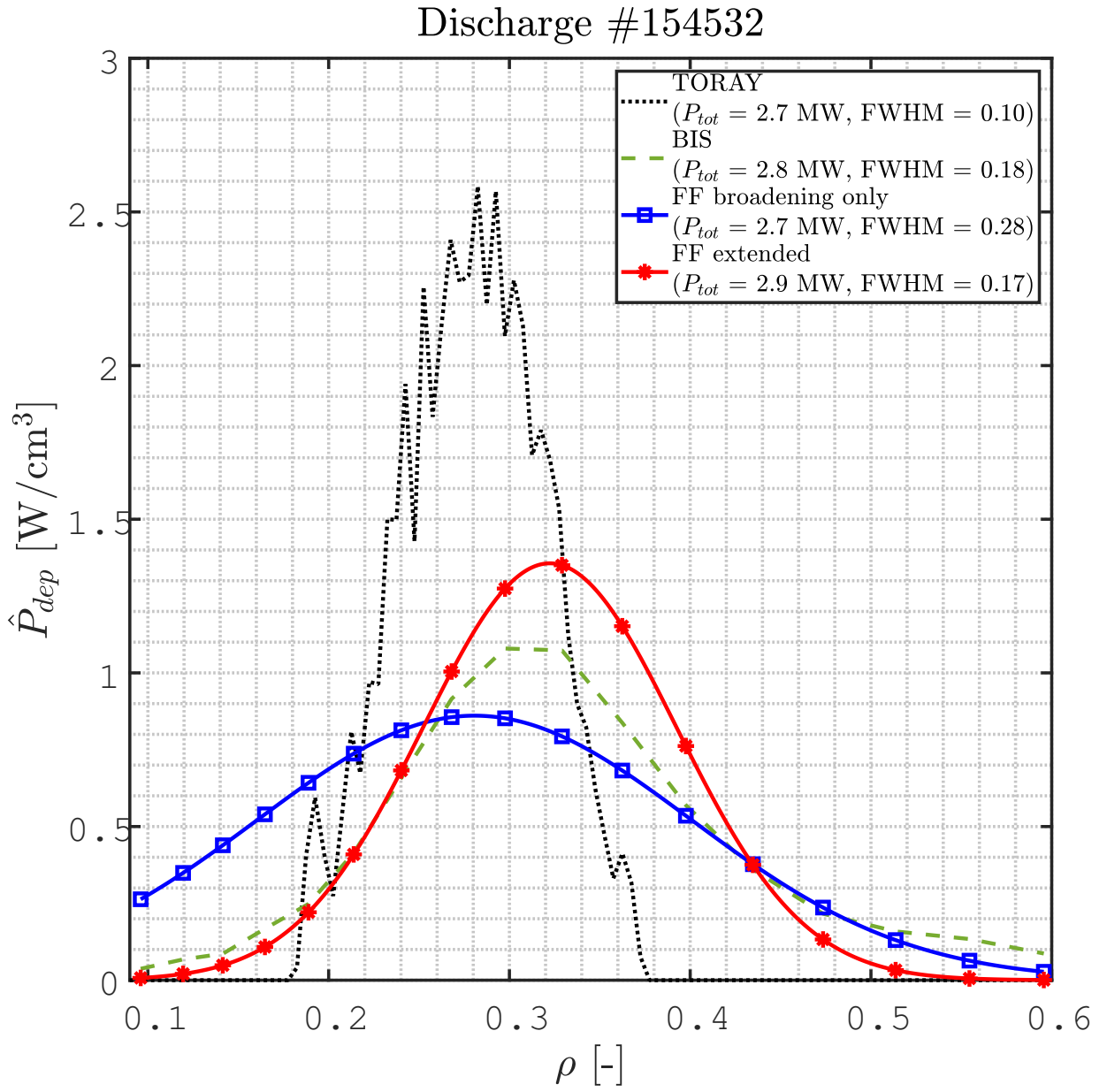
This is the author's peer reviewed, accepted manuscript. However, the online version of record will be different from this version once it has been copyedited and typeset.

PLEASE CITE THIS ARTICLE AS DOI: 10.1063/5.0069869



This is the author's peer reviewed, accepted manuscript. However, the online version of record will be different from this version once it has been copyedited and typeset.

PLEASE CITE THIS ARTICLE AS DOI: 10.1063/5.0069869



This is the author's peer reviewed, accepted manuscript. However, the online version of record will be different from this version once it has been copyedited and typeset.

PLEASE CITE THIS ARTICLE AS DOI: 10.1063/5.0069869

Discharge #165078

